Biosynthesis of Zinc Oxide (ZnO) Using Culture Biomass of *Aspergillus Niger* : The Influence of pH On Textile Morphology And Antimicrobial Activity

Yetria Rilda (yetriarilda@yahoo.com)
Faculty Mathematics and Natural Sciences of Andalas University
Rifki Rinaldi
Faculty Mathematics and Natural Sciences of Andalas University
Syukri Syukri
Faculty Mathematics and Natural Sciences of Andalas University
Armaini Armaini
Faculty Mathematics and Natural Sciences of Andalas University
Refinel Refinel
Faculty Mathematics and Natural Sciences of Andalas University
Anthoni Agustien
Faculty Mathematics and Natural Sciences of Andalas University
Hilfi Pardi
Faculty of Teacher Training and Education Raja Ali Haji Maritime University

Research Article

Keywords: Biosynthesis, ZnO, Enzymatic, Morphology, Aspergillus niger

Posted Date: August 11th, 2021

DOI: https://doi.org/10.21203/rs.3.rs-793590/v1

Abstract

The biosynthesis of zinc oxide (ZnO) is performed through enzymatic mechanisms, by controlling the particle size and morphology of the compound using the sol-gel method. Furthermore, this method utilizes stabilizer obtained from the cell biomass of *Aspergillus niger* bacteria, in order to yield homogeneous and consistent products, which corresponds with the XRD outcome that exhibits good crystallinity. The evaluation of functional, morphological, and antibacterial activities was carried out at pH 6.0-13.0, as the prepared samples were characterized by FT-IR. The analysis showed the interaction of hydroxyl groups, aromatic rings, as well as N-H and O-Zn-O compounds at a wavenumber of 401-584 cm^{-1}. The XRD and SEM characterizations showed that the structure and crystal phase of ZnO were hexagonal wurtzite at dimensions of 36.2 - 45.4 nm. The differences in pH also influenced the dimensions, morphology, and antimicrobial activity. ZnO with pH of 8.0 was characterized by FESEM-EDAX, based on the analysis of morphological uniformity. This characterization obtained rod and cube structures, with atomic ratios of Zn = 61.5% and O = 38.5%. The UV-DRS spectrum showed that the optical band gap was not significantly influenced by the pH of the reactant solution, with a value of Eg = 3.00–3.11 eV. The differences in morphology further distinguished anti-bacterial properties on textile fibres, through the use of the Gram-negative and positive bacteria (*Pseudomonas aeruginosa* and *Staphylococcus aureus*), with inhibition zones of 17-21 mm and 21-25 mm, respectively. Therefore, ZnO is classified as a very strong antibacterial material compared to amoxicillin, with an inhibition zone of 13.6 mm.

Introduction

The technology used to modify the dimensions and morphology of nano-sized material provides great opportunities due to its application in various fields, such as catalysts, sensors, biomedicine, pharmaceutical, medical, cosmetic, food, textile, electronics, oil industry, industrial fertilizers, etc [1–8]. This modification is found to have attracted the attention of many industries, because of the great importance of the metallic raw material and its oxides, having several advantages. The compound is often used, specifically to improve mechanical, physical, and chemical properties, compared to other bulk material [8].

The importance of the synthesis method used, include the production of unique physicochemical and morphological characteristics of a nanomaterial [9]. A new development in this method, involve the use of additives from natural materials, such as plants and microorganism cells, which are more effective, inexpensive, and environmentally friendly. In addition, the use of several plant extracts and microorganisms as additives in the process of synthesizing nanomaterials is known as green chemistry [10].

This study further exploit the use of microorganisms as nanofactories, which are economical, non-toxic, and environmentally friendly for the biosynthesis of nanomaterials [11, 12]. Furthermore, the synthesis mechanism is explained based on the enzymatic reaction of the active components within the

microorganism cells. Several previous studies have also successfully used *Bacillus cereus* and *Rhodopseudomonas capsulate* bacteria for Ag-NPs and Au-NPs synthesis, respectively [13, 14]. The study of Khan *et al*. (2016), utilized the culture of *Bacillus amyloliquefaciens* for TiO_2-NPS synthesis, in order to increase the photocatalytic activity on the degradation of sulfonated textile dyes Reactive Red 31 [15].

Zinc oxide is a semiconductor compound that functions as a photocatalyst, and also have a strong antimicrobial activity for several pathogenic bacteria [16]. Furthermore, the study of Lakshmi *et al.* (2012), determined the antibacterial activity of ZnO against bacteria and fungi, such as *Escherichia coli, Salmonella typhi, Bacillus subtilis, Staphylococcus aureus*, and *Pseudomonas aeruginosa* [16]. Zinc oxide is also a textile coating material that is used to modify the surface of anti-microbial fibres, due to the test results on pathogenic bacterial and fungal cells, such as *Pseudomonas aeruginosa, Eschericia coli, Staphylococcus aureus, Staphylococcus epidermis, Bacillus subtilis, Sacharomyces cerevisae, Penicillium* sp., and *Aspergillus niger* [17–25].

Based on this study, the modification of ZnO synthesis method is carried out by using additives, which are derived from the biomass culture of *A. niger* fungal cell. The mechanism of ZnO biosynthesis is also understood based on the enzymatic reaction structure (nitrate reductase) and stabilizer contributed by the active compound of the fungal cell intracellular enzymes, which functions as capping agents [26]. Several intracellular enzymes, including catalase, lyase, transferase, oxidoreductase, hydrolase, isomerase, and ligase, have the amino acids cysteine, tyrosine, and tryptophan, which also possesses N-terminals within the polypeptide structure functioning as stabilizers. The mechanism of ZnO biosynthesis based on the intracellular structure of *A. niger* cell biomass is shown in the reaction cycle on Fig. 1 [27, 28].

This study also focuses on the biosynthesis of ZnO based on the pH difference of the reactants, in order to optimize the function of intracellular enzymes towards the reduction of Zn^{2+} to Zn^0 and other stabilizers in crystal formation. The pH parameter controls the optimization of ZnO, based on the hydrolysis of the $Zn(NO_3)_2$ precursor, formation of the $Zn(OH)_2$ precipitate core, and stability of crystal growth with controlled dimensions and morphology [29]. Therefore, the ZnO synthesis using microbial cells provide an opportunity to explore its morphology, dimensions, and related properties, towards the utilization in environmental applications. It is also necessary to clearly understand that this biological interaction has electronic properties, reactivity, and affinity, with the contribution to its functionality [30, 31].

Materials And Methods

2.1. Aspergillus niger and its growing conditions

The fungal cells of *A. niger* were obtained from the Biota Laboratory of Andalas University, as the process and growth conditions of the subculture were carried out on Potato Dextrose Agar (PDA) media, at 32°C for 72 h [23].

2.2. Nanostructured materials

The biosynthesis process was carried out by dissolving 1.626 g of ZnO seeds in distilled water, and deposited for 24 h. Furthermore, the precipitate was dried at 100°C and coated on a glass substrate, as the precursor mixture containing zinc nitrate ($Zn(NO_3)_2$) and sodium hydroxide (NaOH) in a ratio of 2:1 was dissolved in distilled water, and stirred until homogeneous. Also, 1.2 g of dry biomass and 1.457 g of CTAB were added, as the pH of the reactant solution was set to 6.0, 8.0, 10.0, and 13.0, then homogenized at 400 rpm for 4 h. Based on this condition, the obtained white precipitate was dried at 110°C for 3 h in an oven, coated on a glass substrate after ZnO seeds, and calcined at 600°C for 4 h [22].

2.3 Applications on Textile Fibers

The coating of 8 x 8 cm textile materials with ZnO was carried out by a dip-spin approach. These materials were previously washed with 2g/L detergent, dipped in Na_2CO_3 solution, and rinsed with distilled water. Based on this condition, the textiles were further coated with a solution of citric acid and Na_2HPO_2. Furthermore, these materials were coated with ZnO suspension, and dried at 80°C for 5 mins. This ZnO coating was carried out repeatedly, as the remaining uncoated fibres were washed with distilled water, and dried at 80°C for 10 mins [22].

2.4 Evaluation of Textile Antibacterial Activity

Textiles with a diameter of 0.6 cm were tested for anti-bacterial properties, by using *Staphylococcus aureus* and *Pseudomonas aeruginosa* bacteria, as these isolates were inoculated on Potato Dextrose Agar (PDA) media in a petri-dish container. Furthermore, the textile pieces were positioned on the bacterial inoculation section, as the petri-dish plate was further incubated at UV irradiation (λ) of 385–400 nm. The observation of the inhibition zone was also carried out every 24–96 h [22].

2.5 Instrumentation and Data Analysis

The morphology of the biosynthetic ZnO was characterized by using the FESEM-EDAX (Field Emission Scanning electron microscopy-dispersive X-ray spectroscopy) instrument, as the crystal structure and dimensions were determined by the X-ray diffraction (XRD). Furthermore, the Fourier Transform Infrared (FT-IR) spectra and Ultraviolet-Differential Reflectance Spectroscopy (UV-DRS) were used for the identification of functional groups and optical properties analysis, respectively.

Results And Discussion

3.1 Analysis of Fourier Transform Infra Red (FT-IR)

The mechanism for the ZnO formation at different biosynthetic pH should present similar steps to Fig. 1 [27], as the first reaction was related to the solubility of the zinc precursor ($Zn(NO_3)_2$), precipitate ($Zn(OH)_2$) core development, and the stability for crystal growth in the presence of a capping agent substitution. Furthermore, Fig. 2 indicates the FT-IR spectrum of ZnO biosynthesis at different pH, as the analysis showed that there were functional associations at the absorption band intensity of 3385 cm^{-1},

namely the strain vibration of the O-H group [32]. The intensity of 1640 – 1635 cm^{-1} was also the strain vibration of N-H bond, which was obtained from the amino acids of *A. niger* intracellular enzymes. Also, the methyl group (-CH_3) of the surfactant CTAB (Cetyltrimethyl ammonium bromide) was used as a template for the formation of ZnO nanorods. The absorption band intensity at ~ 860 cm-1 was also Zn–OH, which was obtained from the hydrolysis of $Zn(NO_3)_2$ precursor in the pH medium of 6.0–13.0. However, the intensity of 584–401 cm^{-1} was indicated as an O-Zn-O group [33].

The morphological pattern of ZnO formed adjusted to the pH of the biosynthetic media (6.0–13.0), due to the difference in the intensity of the absorption band produced from each functional group. Furthermore, Fig. 2a indicated the spectrum of ZnO biosynthesis in a slightly acidic medium (pH = 6.0), as the absorption intensity of N-H and O-H was lower in the basic channel. The $Zn(NO_3)_2$ precursor was not completely hydrolyzed at the conditions of pH = 6.0, as the Zn^{+2} ion precipitation into $Zn(OH)_2$ was unstable. More energy was also needed for phase transitions in the formation of ZnO nanostructures [34]. Furthermore, Figs. 2b and 2c represented the ZnO biosynthesis at pH = 8.0 and 10.0, respectively, as the spectrum showed that the intensity of the absorption band was greater at a wavenumber of 584–401 cm^{-1}. The crystal formed was also observed to be more stable, due to being indicated by a larger amount of substituted NH, which served as a stabilizer for the growth of ZnO. This was indicated by the higher intensity of absorption band at 1640 – 1635 cm^{-1}. Based on being associated with the optimum pH, the growth of *A. niger* cells occurred at pH 8.0–10.0, due to being more productive in providing intracellular enzymes as reducing agents and stabilizers, within the ZnO biosynthesis process [28]. Furthermore, Fig. 2d showed the biosynthetic spectrum of ZnO in a strongly alkaline medium of pH = 13.0. Based on this condition, excess OH^- ions and Zn^{+2} formed a very stable $Zn(OH)_2$ precipitate, as the N-H ligand was difficult to substitute. Excess OH^- ions were also moisturized on the ZnO surface, in order to form hydrated zinc oxide. When correlated with the XRD spectrum in Fig. 3, the biosynthesis at pH = 13.0 was indicated by the new intensity of hydrated Zn-O, at 2θ = 29.37° [23, 27, 29].

3.2 X-Ray Diffraction (XRD)Analysis of ZnO

The XRD pattern of ZnO was observed at the biosynthetic pH of 6.0–13.0, as shown in Fig. 3. Furthermore, the intensity at 2θ = 31.74°, 34.40°, 36.23°, 47.53°, 56.59°, 62.86°, 66.38°, 67.96°, and 69.10°, were the specific intensities of the ZnO wurtzite crystal structure, with hkl planes of 100, 002, 101, 102, 110, 200, 112, and 201 as hexagonal cell units, based on the ICSD-155780 standard [35]. The highest intensity was generally categorized as ZnO wurzite at similar 2θ, except in Fig. 3. Based on the ZnO biosynthesis at pH = 13.0, a new peak at 2θ = 29.37° was obtained, which indicated the intensity of hydrated Zn-O based on the standard of ICSD-15008. The study of Karuna et al. (2018), reported that the intensity at 2θ = 29.37° was hydrated ZnO, which was formed at a strong alkaline pH of 13.5 [35]. According to McBride et al. (2003) and Podlogar et al., the optimal condition of ZnO synthesis occurred at pH = 8.0–12.9. Based on this condition, the solubility of Zn ions was more saturated to form $Zn(OH)_2$

precipitate, as ligand substitution (NH) formed coordination $[Zn(OH)_2(NH_3)_4]$ and a stable $Zn(OH)_4^{2-}$ core. Mean while, ZnO crystal growth was more directed [36, 37].

Based on the Debye Scherer equation, the data in Table 1 showed the size and phase of ZnO crystals, due to differences in biosynthetic pH (6.0–13.0). These influenced the ZnO dimensions, as higher pH levels produced greater amount of OH^- ion concentration, and more stable $Zn(OH)_2$ precipitate formation. Furthermore, the substitution of amine ligands in the precipitate was more difficult towards stabilizing the core formation and crystal growth of ZnO, as described in Fig. 2 [35]. The optical absorption rates in Table 1 were also used for the electronic transition analysis between bands, bandgap widths, and orbitals. Additionally, the contribution of defects to these transitions was highly dependent on particle size, which influenced the ability of ZnO to absorb UV light. The small value of the energy gap also enabled ZnO to easily absorb Ultraviolet light [38].

Table 1
ZnO crystal dimensions based on differences in biosynthetic pH

ZnO-NS	Ukuran Kristal (nm)	Energi gap (eV)
pH 6.0	38.2	3.01
pH 8.0	36.2	3.00
pH 10.0	45.4	3.03
pH 13.0	41.4	3.01

The XRD data were further refined through the Le Bail refinement technique, by using Rietica software to descriptively determine the crystal structure (Fig. 4 and Table 2). Based on Fig. 4, the XRD patterns were used to observe the crystal structure on Table 1, as the Le Bail refinement was carried out on the data. Furthermore, the structural parameters of ZnO phase with P63mc space group ($a = b = 3.25254$ Å, $c = 5.2110$ Å, $\alpha = \beta = 90°$, $\gamma = 120°$) (ICSD-155780) was hexagonal, and also a fairly low fit for all pH parameters. The biosynthesis of all parameters at pH = 6.0–10.0 was further automatically refined to obtain the best fits and the unit cell. However, there was a new peak that did not match the model at pH = 13.0, which indicated the occurrence of a secondary phase that was different from hexagonal ZnO. The pH of 8.0 also had the smallest suitability parameter, compared to those at 6.0, 10.0 and 13.0. This indicated that the biosynthetic conditions at pH = 8.0 were optimal in obtaining the hexagonal structure of ZnO.

Table 2
Refined structural parameters of ZnO sample obtained from XRD

	ZnO pH 6	ZnO pH 8	ZnO pH 10	ZnO pH 13
Space Group	$P6_3mc$	$P6_3mc$	$P6_3mc$	$P6_3mc$
Z	2	2	2	2
a (Å)	3.2502	3.2481	3.2510	3.2519
c (Å)	5.2067	5.2037	5.2084	5.2076
V(Å^3)	47.6365	47.5473	47.6755	47.6941
Rp	5.87	5.88	6.80	8.04
Rwp	7.72	7.36	9.47	13.7
χ2	1.60	1.55	2.55	5.20

3.4 Analysis of ZnO Morphology

Figure 5 indicates the ZnO morphology from Scanning Electron Microscopy (SEM) analysis, with 5a showing the biosynthesis at pH = 8.0, where a small crystal size was produced based on the measurement of XRD data. The dominant morphologies observed were rods, which had high uniformity degrees. Furthermore, Fig. 5b shows biosynthesis at pH = 10.0 and 13.0, where a rod-like morphology and mixed plate structure were produced, respectively. The spheric morphology with low uniformity is also presented in Fig. 5c, as FESEM-EDAX characterization was carried out with a high resolution at pH = 8.0, in order to obtain clearer information on the results produced. Figure 6 further indicates that there are rods and cubes with higher uniformity levels of ZnO nanorods distribution.

The differences in biosynthetic pH produced several ZnO morphology and uniformity distribution of particle size, which in turn influenced the amount of N-H substituted for the crystal nucleation stabilizer [33, 39]. Furthermore, the study of Alias et al. (2010), reported the agglomeration of alkaline media synthesis with pH greater than 12. This was due to the more difficult substitution of stabilizer in $Zn(OH)_2$ precipitate [40, 41]. Based on EDAX analysis, ZnO contained the atomic composition of Zn = 61.5% and O = 38.5%.

3.5 ZnO application as textile coating

The aim of ZnO coating on textile fibres was to modify the function of anti-bacterials. This was due to using citric acid as a crosslinker, based on the formation of covalent ester interactions between the fibres and ZnO [42]. Furthermore, reported that covalent ester interactions were characterized by FT-IR, due to the absorption band intensity of the C = O group at wave number 1643–1456 cm^{-1}. The intensity of 3324–3414 cm^{-1} was also the OH strain vibration obtained from the cellulose of the textile materials.

Additionally, there was a difference between the intensity of the C = O group on textiles, without coating with ZnO materials [22, 23, 26, 33].

Figure 7 indicates the Scanning Electron Microscopy (SEM) analysis of a textile material, which is coated with ZnO. Based on the use of a crosslinked, the ZnO powder evenly spreads on all parts of the coated fibres. This coating stability was tested based on repeated washing, which occurred between 5–10 times [42]. According to the EDX analysis, the composition of ZnO-coated textiles is C = 60.72 %, O = 33.37 %, and Zn = 5.91 %.

3.6 Evaluation on antibacterial activity of the nanofinished textiles

The evaluation of ZnO anti-bacterial activity on textile fibres was carried out in vitro, on *Staphylococcus aureus* and *P. aeruginosa*, as the data of the inhibition zone measurement based on the differences in biosynthetic pH are shown in Figs. 8 and 9. Based on Fig. 9, the comparison of the ZnO inhibition zone at pH = 6.0–13.0, is observed against the two bacterial species. Furthermore, these figures (Figs. 8 and 9) indicated that the inhibition ability of *P. aurigenosa* bacteria was more effective than *S. Aureus*, at pH = 8.0. The observation of growth area was also carried out with petri-dish photos, by using the Image pro Analyzer analysis system (cm^2/day) for 3 days, at 24, 48, and 96 h. This was conducted in order to determine the bacteria behaviour against the presence of ZnO. The variation was because the two bacterial species had different cell wall thicknesses. Furthermore, the *P. aurigenosa* is a Gram negative bacteria with a cell wall layer of 30 A°, which was thinner than that of the *S. aureus* Gram positive at 250 A°. The cell wall layer of *S. aureus* also contained teichoic acid [21]. Differences in inhibition ability were further influenced by dimensions, morphology, and time [43]. Additionally, the ZnO activity test obtained an inhibition zone of > 20 mm, at different pH and observation time of 24–96 h. Therefore, ZnO is a very strong anti-bacterial agent for a number of pathogenic bacteria, due to the inhibitory abilities of the utilized species. This is superior to amoxicillin, which is found at an inhibition zone of 13.6 mm [22, 23].

Conclusion

ZnO biosynthesis using *A. niger* biomass optimized the crystal growth mechanism through pH regulation. This was due to having the smallest dimension of 36.17 nm with rods morphology at pH = 8.0, as well as a high uniformity level and antibacterial activity. Furthermore, the XRD characterization and Le Bail refinement were performed with the structural parameters of the ZnO phase and P63*mc* space group model ($a = b = 3.25254$ Å, $c = 5.2110$ Å, $\alpha = \beta = 90°$, $\gamma = 120°$). The results showed that ZnO had a hexagonal wurtzite structure, with a similarity number close to the model at ZnO pH = 8.0 nm. Also, ZnO anti-bacterial activity on textile fibre media had very strong inhibitory power against gram (+ and -) of *Staphylococcus aureus* and *Pseudomonas aeruginosa* bacteria, with inhibition zones of 21.55 and 25.50 mm, respectively. Both species had a zone > 20 mm, and were classified as having a stronger inhibitory ability than amoxicillin, which was at 13.6 mm.

Declarations

Acknowledgement

This research was funded by the Directorate of Resources, Directorate General of Higher Education, Ministry of Education, Culture, and Research and Technology in accordance with Research Contract 104/E4.1/AK.04.PT/2021 12 Juli 2021 dan T/32/UN.16.17/PT. 01.03/PD Material Maju/2021 13 Juli 2021

References

1. L.J. Frewer, N. Gupta, S. George, A.R.H. Fischer, E.L. Giles, D. Coles, Trends Food Sci. Technol. **40**, 211 (2014)
2. L. Syedmoradi, M. Daneshpour, M. Alvandipour, F.A. Gomez, H. Hajghassem, K. Omidfar, Biosens. Bioelectron. **87**, 373 (2017)
3. A.K. Hussein, Renew. Sustain. Energy Rev. **62**, 767 (2016)
4. A. Bera, H. Belhaj, J. Nat. Gas Sci. Eng. **34**, 1284 (2016)
5. M. Ayelén Vélez, M. Cristina Perotti, L. Santiago, A. María, Gennaro, E. Hynes, *Bioactive Compounds Delivery Using Nanotechnology: Design and Applications in Dairy Food* (Elsevier Inc., 2017)
6. M.K. Sharif, F.-H. Shah, M.S. Butt, H.R. Sharif, *Role of Nanotechnology in Enhancing Bioavailability and Delivery of Dietary Factors* (Elsevier Inc., 2017)
7. A.K.M.A. Hosne Asif, M.Z. Hasan, Int. J. Curr. Eng. Technol. **8**, 227 (2018)
8. M. Zali, A. Yudi Heryadi, S. Nurlaila, Z. Fanani, Int. J. Adv. Multidiscip. Res **5**, 45 (2018)
9. H. Agarwal, S. Venkat Kumar, S. Rajeshkumar, Resour. Technol. **3**, 406 (2017)
10. H. Agarwal, S. Venkat Kumar, S. Rajeshkumar, Resour. Technol. **3**, 406 (2017)
11. S. Kargozar, M. Mozafari, Mater. Today Proc. **5**, 15492 (2018)
12. M. Ebadi, M.R. Zolfaghari, S.S. Aghaei, M. Zargar, M. Shafiei, H.S. Zahiri, K.A. Noghabi, RSC Adv. **9**, 23508 (2019)
13. A. Prakash, S. Sharma, N. Ahmad, A. Ghosh, and P. Sinha, 2011, 156 (2011)
14. S. He, Z. Guo, Y. Zhang, S. Zhang, J. Wang, N. Gu, Mater. Lett. **61**, 3984 (2007)
15. R. Khan, M.H. Fulekar, J. Colloid Interface Sci. **475**, 184 (2016)
16. V.N. Kalpana, B.A.S. Kataru, N. Sravani, T. Vigneshwari, A. Panneerselvam, and V. Devi Rajeswari, OpenNano **3**, 48 (2018)
17. Y. Chen, H. Ding, S. Sun, Nanomaterials 7, (2017)
18. L. Hiremath, S. Narendra Kumar, P. Sukanya, Mater. Today Proc. **5**, 21030 (2018)
19. P. Kamali, N. Talebian, J. Coatings Technol. Res. **15**, 1133 (2018)
20. T. Yuranova, R. Mosteo, J. Bandara, D. Laub, J. Kiwi, J. Mol. Catal. A Chem. **244**, 160 (2006)

21. A. Verbič, M. Gorjanc, B. Simončič, Coatings **9**, 17 (2019)
22. Y. Rilda, D. Damara, Y.E. Putri, R. Refinel, A. Agustien, H. Pardi, Heliyon (2020)
23. Y. Rilda, D. Dwiyanti, S. Syukri, A. Agustien, H. Pardi, J. Dispers. Sci. Technol. **0**, 1 (2020)
24. F.S. Al-khattaf, Saudi. J. Biol. Sci. **28**, 3624 (2021)
25. N. Pantidos, J. Nanomed. Nanotechnol. 05, (2014)
26. V.N. Kalpana, B.A.S. Kataru, N. Sravani, T. Vigneshwari, A. Panneerselvam, and V. Devi Rajeswari, OpenNano **3**, 48 (2018)
27. N. Mahmoudi Khatir, Z. Abdul-Malek, A.K. Zak, A. Akbari, F. Sabbagh, J. Sol-Gel. Sci. Technol. **78**, 91 (2016)
28. A. Rajan, E. Cherian, G. Baskar, Int. J. Mod. Sci. Technol. **1**, 52 (2016)
29. Y. Rilda, D. Damara, Y.E. Syukri, Putri, Refinel, A. Agustien, IOP Conf. Ser. Earth Environ. Sci. **217**, 0 (2019)
30. A.E. Nel, L. Mädler, D. Velegol, T. Xia, E.M.V. Hoek, P. Somasundaran, F. Klaessig, V. Castranova, M. Thompson, Nat. Mater. **8**, 543 (2009)
31. S. Aula, S. Lakkireddy, A.V.N. Swamy, A. Kapley, K. Jamil, N.R. Tata, K. Hembram, Mater. Res. Express **1**, 0 (2014)
32. A.A.M. Sakib, S.M. Masum, J. Hoinkis, R. Islam, M.A.I. Molla, J. Compos. Sci. **3**, 91 (2019)
33. S.H. Ribut, C.A. Che Abdullah, M. Mustafa, M.Z. Mohd, Yusoff, S.N. Ahmad, Azman, Mater. Res. Express **6**, 25016 (2019)
34. M.F. Kasim, N. Kamarulzaman, R. Rusdi, A.A. Rahman, J. Phys. Conf. Ser. 1083, (2018)
35. K.P. Ghoderao, S.N. Jamble, R.B. Kale, Optik (Stuttg). **156**, 758 (2018)
36. R.A. McBride, J.M. Kelly, D.E. McCormack, J. Mater. Chem. **13**, 1196 (2003)
37. M. Podlogar, A. Rečnik, G. Yilmazoglu, I. Özer, M. Mazaj, E. Suvaci, S. Bernik, Ceram. Int. **42**, 15358 (2016)
38. N. Tio-sio-chitosan, Y. Rilda, A. Meranti, Y. Citra, R. Refinel, Y.E. Putri, A. Agustien, H. Pardi, Mater. Res. Innov. **00**, 1 (2020)
39. S.S. Alias, A.B. Ismail, A.A. Mohamad, J. Alloys Compd. **499**, 231 (2010)
40. Y. Miyake, T. Iwai, M. Sugai, K. Miura, H. Suginaka, N. Nagasaka, J. Dent. Res. **70**, 1045 (1991)
41. C.K. Stover, X.Q. Pham, A.L. Erwin, S.D. Mizoguchi, P. Warrener, M.J. Hickey, F.S.L. Brinkman, W.O. Hufnagle, D.J. Kowallk, M. Lagrou, R.L. Garber, L. Goltry, E. Tolentino, S. Westbrock-Wadman, Y. Yuan, L.L. Brody, S.N. Coulter, K.R. Folger, A. Kas, K. Larbig, R. Lim, K. Smith, D. Spencer, G.K.S. Wong, Z. Wu, I.T. Paulsen, J. Relzer, M.H. Saler, R. E. W. Hancock, S. Lory, and M. V. Olson, Nature **406**, 959 (2000)
42. Y. Rilda, A. Meranti, Y. Citra, R. Refinel, Y.E. Putri, A. Agustien, H. Pardi, Mater. Res. Innov. (2020)
43. S. Rajeshkumar, Resour. Technol. **2**, 30 (2016)

Figures

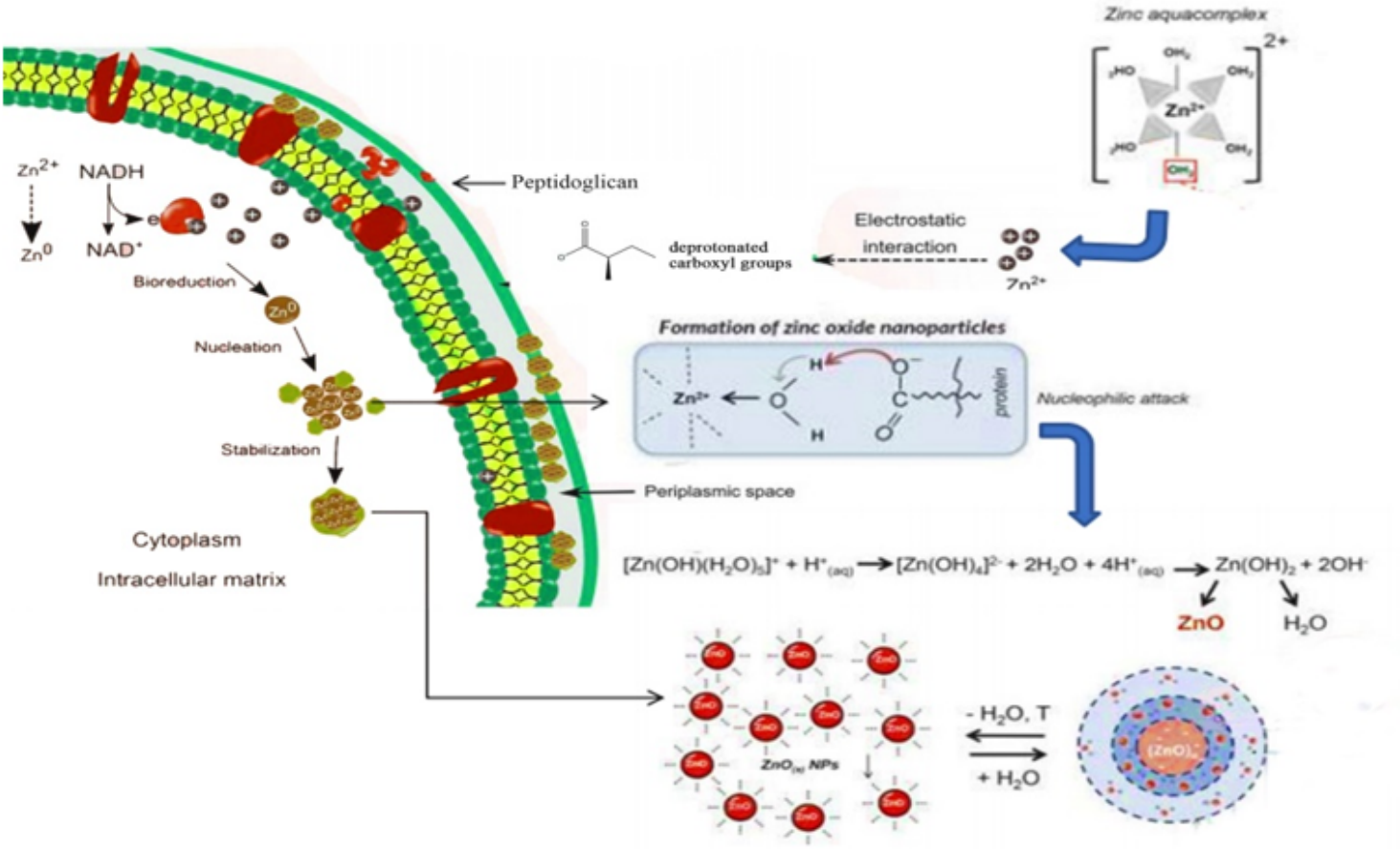

Figure 1

Intracellular mechanism of ZnO biosynthesis

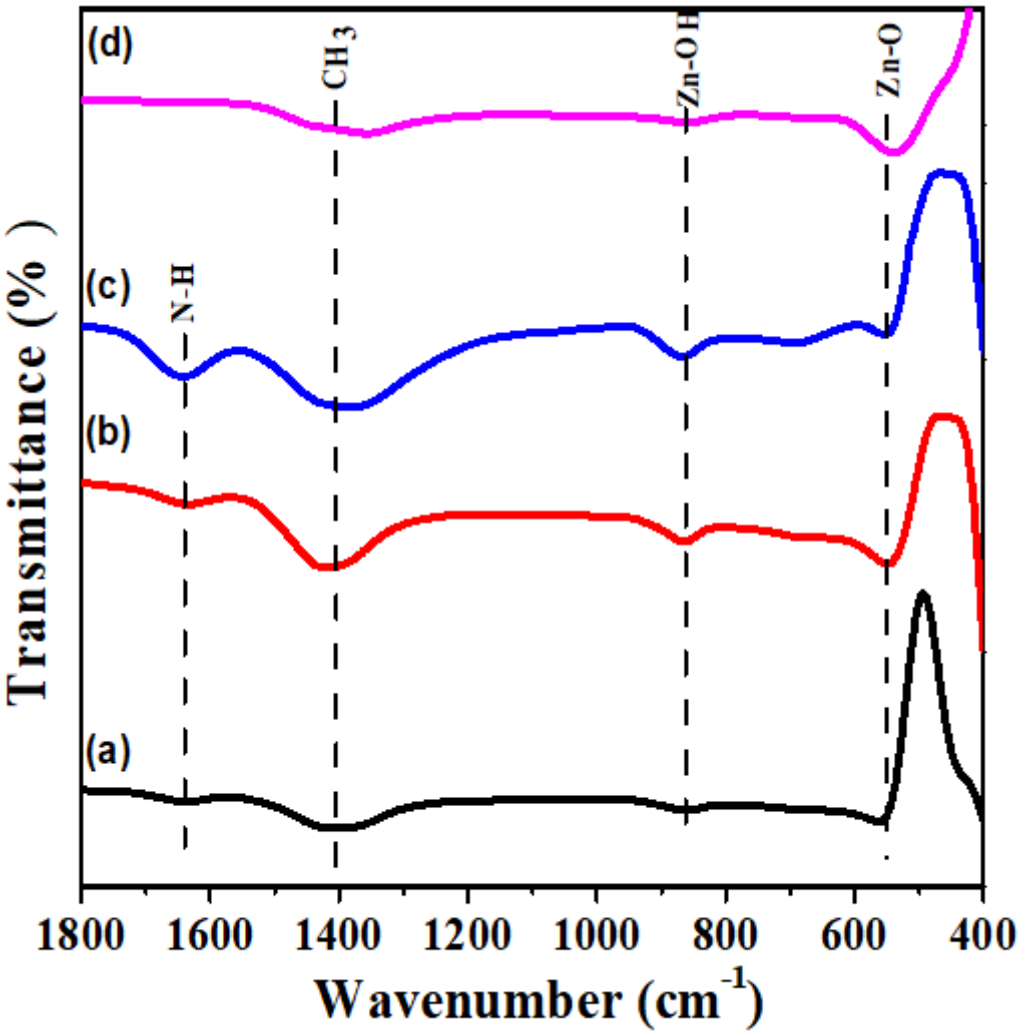

Figure 2

ZnO FTIR spectrum from biosynthesis at (a). pH = 6.0, (b). pH = 8.0, (c). pH = 10.0 and (d). pH = 13.0.

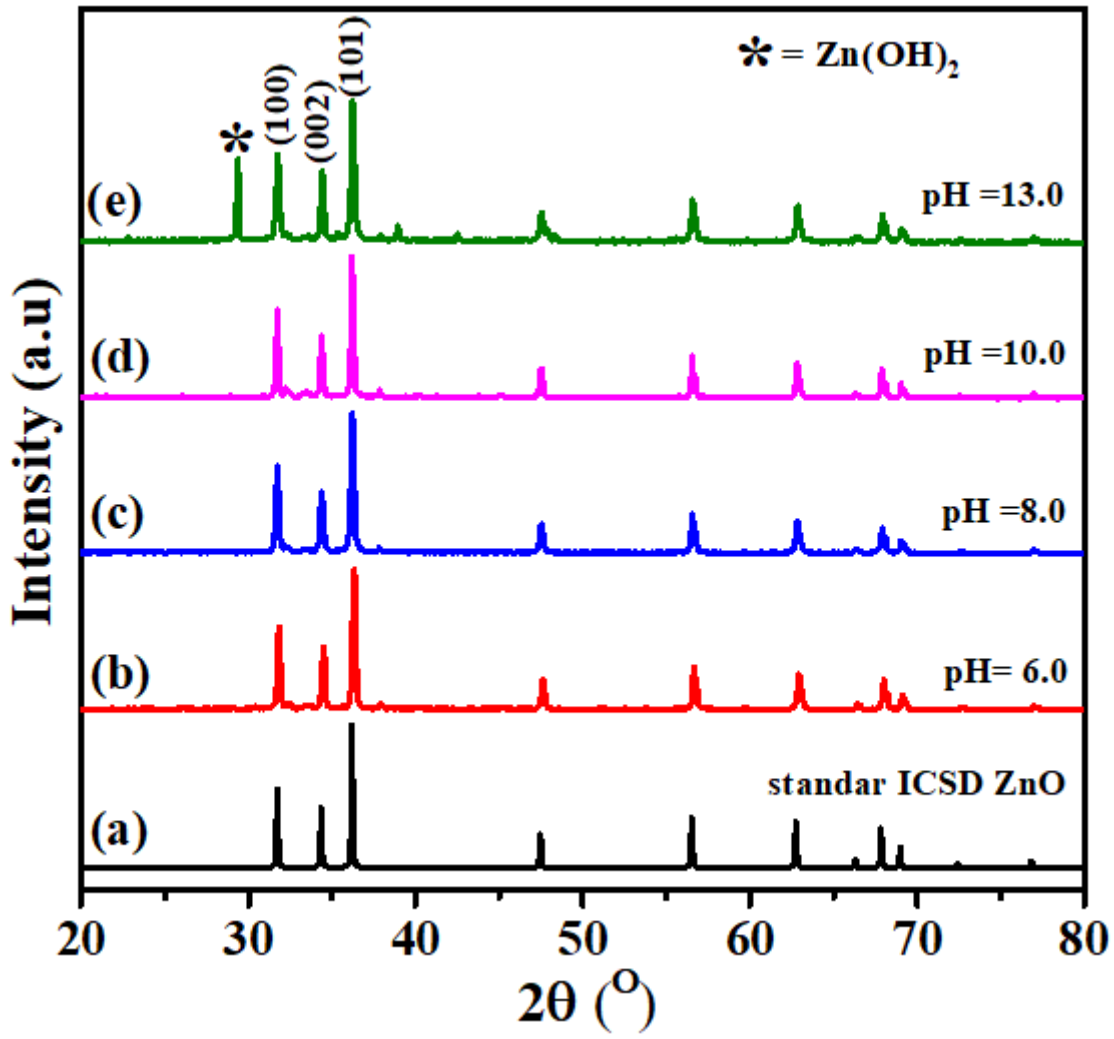

Figure 3

XRD pattern of ZnO Powder (a). standard ZnO (ICSD -155780), biosynthetic (b). pH = 6.0, (c). pH = 8.0, (d). pH = 10.0 and (e). pH = 13.0

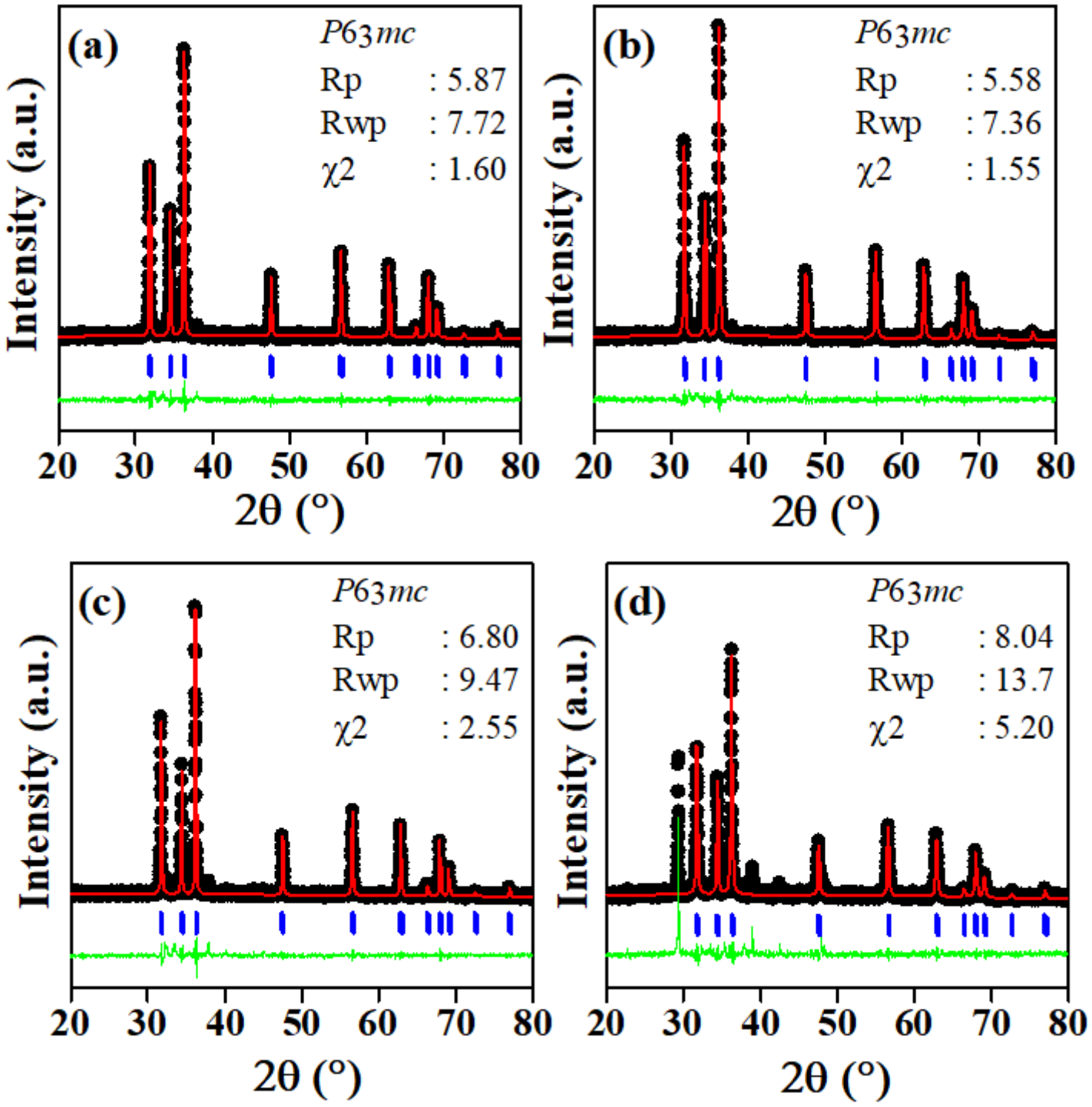

Figure 4

LeBail refinement Plot of ZnO at (a) pH 6.0 (b) pH 8.0 (c) pH 10.0 and (d) pH 13.0

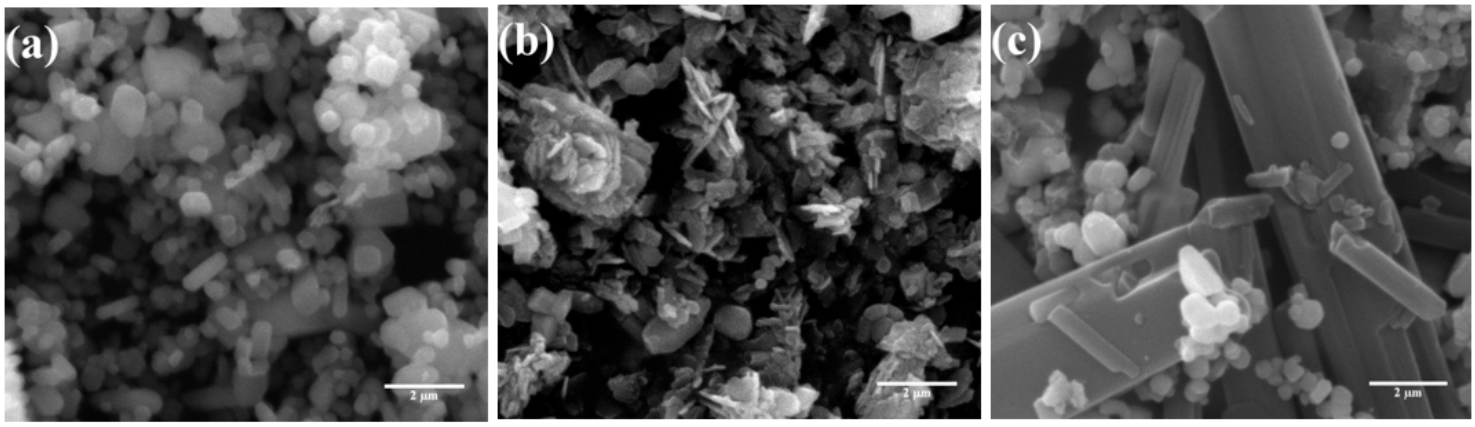

Figure 5

SEM pattern of ZnO-NPs morphology (a). pH=8.0, (b) pH =10.0 and (c) pH = 13.0

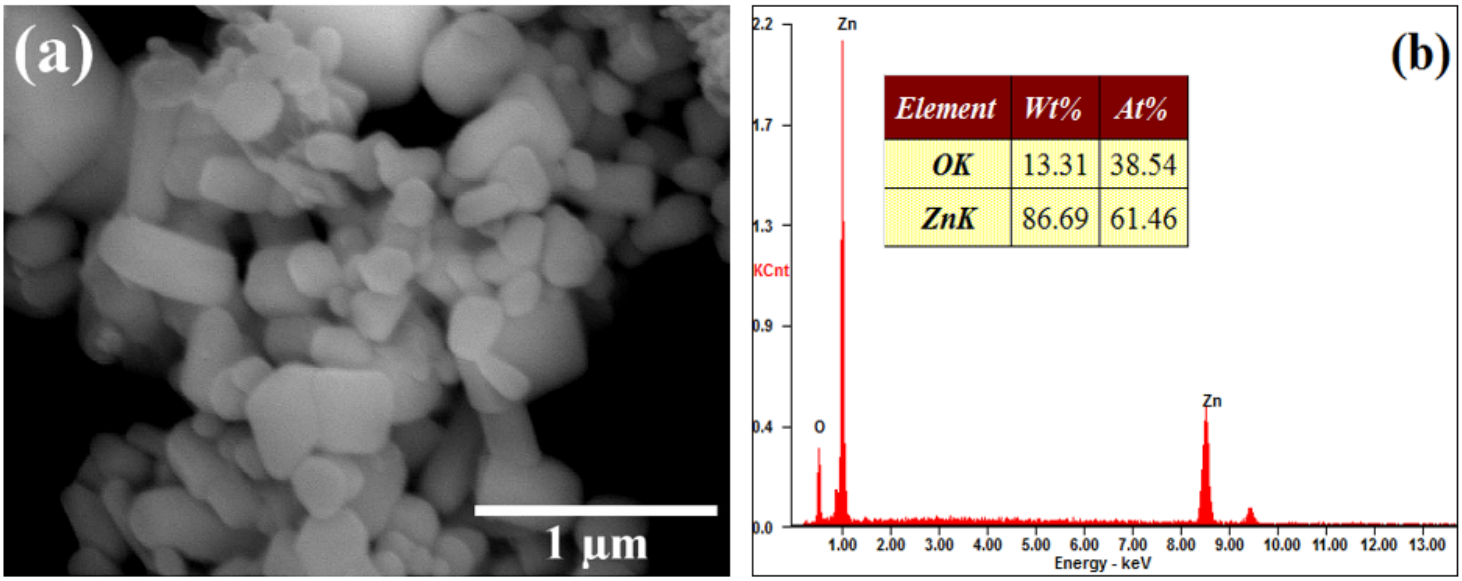

Figure 6

FE-SEM analysis at pH = 8.0. (a) Particle distribution pattern and (b) EDAX analysis

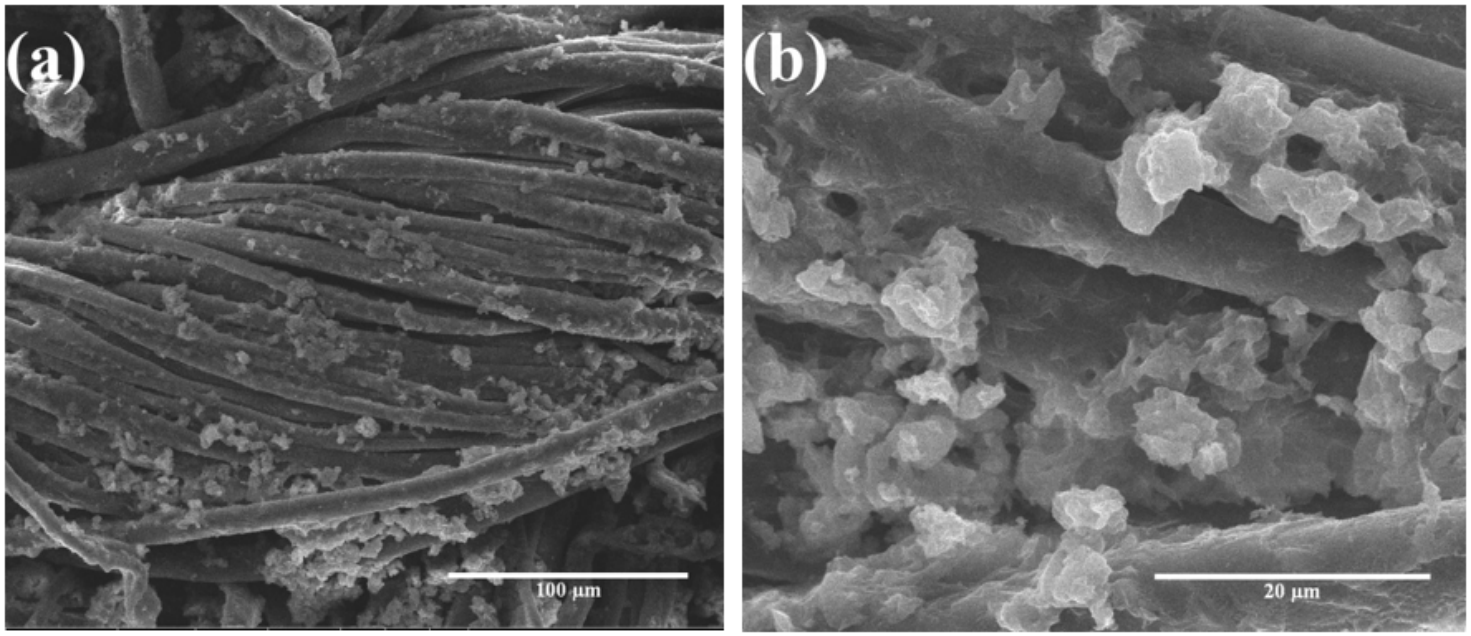

Figure 7

SEM analysis on textile fiber material coated with ZnO at a magnification of 5000 and 10,000 times

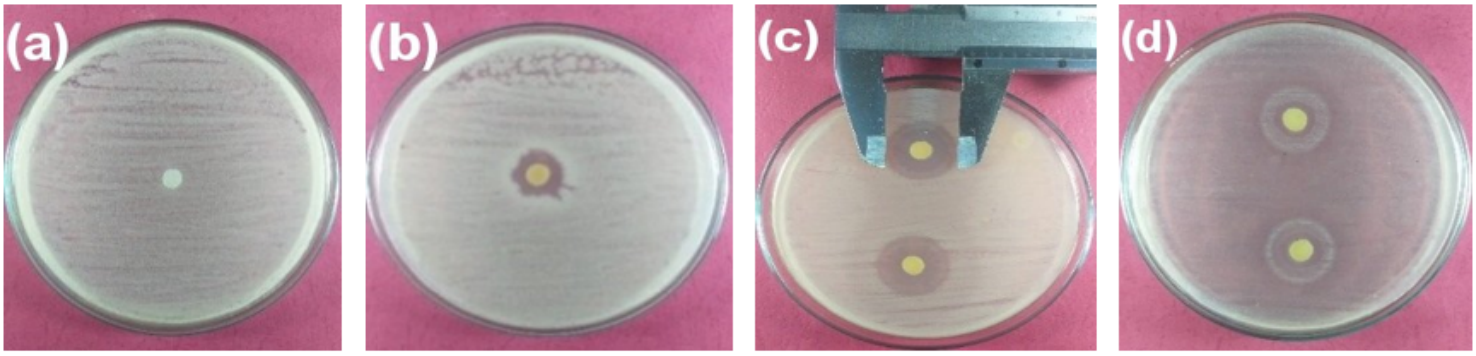

Figure 8

Bacterial inhibition zones on textile fiber coated with ZnO at pH= 8.0 (a) control (-), (b) control (+), (c) Staphylococcus aureus (d) Pseudomonas aeruginosa

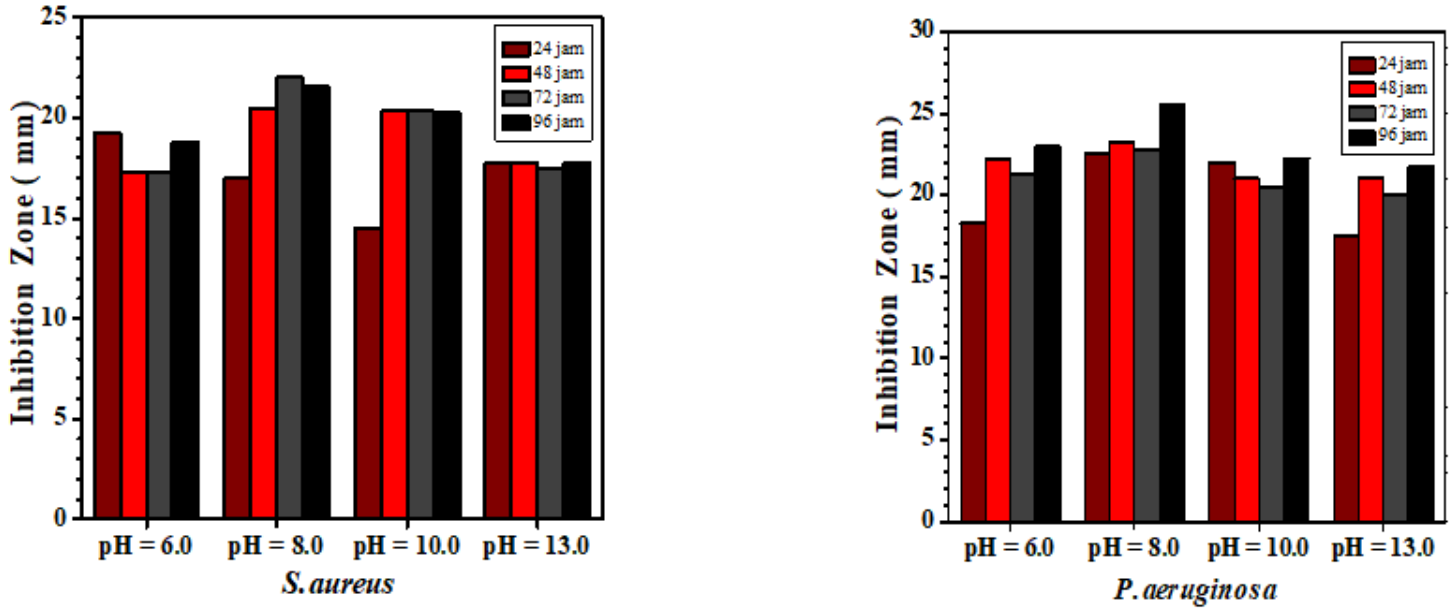

Figure 9

ZnO inhibition zones on textile fiber media (a) control (-), (b) control (+), (c) S. aureus (d) P. aeruginosa